Investigation of optical currents in coherent and partially coherent vector fields

Angelsky, O. V.; Gorsky, M. P.; Maksimyak, P. P.; Maksimyak, A. P.; Hanson, Steen Grüner; Zenkova, C. Yu.

Published in:
Optics Express

Link to article, DOI:
10.1364/OE.19.000660

Publication date:
2011

Document Version
Publisher's PDF, also known as Version of record

Investigation of optical currents in coherent and partially coherent vector fields

O. V. Angelsky,[1,*] M. P. Gorsky,[1] P. P. Maksimyak,[1] A. P. Maksimyak,[1] S. G. Hanson,[2] and C. Yu. Zenkova[3]

[1]*Department of Correlation Optics, Chernivtsi National University,2, Kotsyubinsky Str., Chernivtsi 58012, Ukraine*
[2]*DTU Fotonik, Department of Photonics Engineering, DK-4000 Roskilde, Denmark*
[3]*Optics and Spectroscopy Department, Chernivtsi National University, 2, Kotsyubinsky Str., Chernivtsi 58012, Ukraine*
**angelsky@itf.cv.ua*

Abstract: We present the computer simulation results of the spatial distribution of the Poynting vector and illustrate motion of micro and nanoparticles in spatially inhomogeneously polarized fields. The influence of phase relations and the degree of mutual coherence of superimposing waves in the arrangements of two-wave and four-wave superposition on the characteristics of the microparticle's motion has been analyzed. The prospects of studying temporal coherence using the proposed approach are made. For the first time, the possibility of diagnostics of optical currents in liquids caused by polarization characteristics of an optical field alone, using nanoscale metallic particles has been shown experimentally.

OCIS codes: (030.1640) Coherence; (120.5410) Polarimetry; (170 4580) Optical diagnostics for medicine; (230.5440) Polarization-selective devices.

References and links

1. M. V. Berry, "Optical currents," J. Opt. A, Pure Appl. Opt. **11**, 094001 (2009).
2. O. V. Angelsky, N. N. Dominikov, P. P. Maksimyak, and T. Tudor, "Experimental revealing of polarization waves," Appl. Opt. **38**(14), 3112–3117 (1999).
3. T. Tudor, "Polarization waves as observable phenomena," J. Opt. Soc. Am. A **14**(8), 2013–2020 (1997).
4. M. V. Berry and K. T. McDonald, "Exact and geometrical optics energy trajectories in twisted beams," J. Opt. A, Pure Appl. Opt. **10**(3), 035005 (2008).
5. M. V. Berry, and M. R. Dennis, "Polarization singularities in isotropic random vector waves," Proc. R. Soc. Lond. A **456**, 2059–2079 (2001).
6. O. V. Angelsky, S. G. Hanson, C. Yu. Zenkova, M. P. Gorsky, and N. V. Gorodyns'ka, "On polarization metrology (estimation) of the degree of coherence of optical waves," Opt. Express **17**(18), 15623–15634 (2009).
7. I. Mokhun, and R. Khrobatin, "Shift of application point of angular momentum in the area of elementary polarization singularity," J. Opt. A, Pure Appl. Opt. **10**(6), 064015 (2008).
8. R. Khrobatin, I. Mokhun, and J. Viktorovskaya, "Potentiality of experimental analysis for characteristics of the Poynting vector components," Ukr. J. Phys. Opt. **9**(3), 182–186 (2008).
9. A. Y. Bekshaev, and M. Soskin, "M.S.Soskin Transverse energy flows in vectorial fields of paraxial light beams," Proc. SPIE, **6729**, 67290G, 67290G-12 (2007).
10. O. V. Angelsky, S. B. Yermolenko, C. Yu. Zenkova, and A. O. Angelskaya, "Polarization manifestations of correlation (intrinsic coherence) of optical fields," Appl. Opt. **47**(29), 5492–5499 (2008).
11. O. V. Angelsky, C. Yu. Zenkova, M. P. Gorsky, and N. V. Gorodyns'ka, "Feasibility of estimating the degree of coherence of waves at the near field," Appl. Opt. **48**(15), 2784–2788 (2009).
12. M. Born, and E. Wolf, Principles of optics. New York: Cambridge University Press (1999)
13. J. Turkevich, P. C. Stevenson, and J. Hillier, "A study of the nucleation and growth processes in the synthesis of colloidal gold // J," Discuss. Faraday Soc. **11**, 55–75 (1951).

1. Introduction

Experimental study and computer simulation of the behavior of small spherical particles embedded in optical fields provides a deeper understanding of the role of the Poynting vector for description of optical currents in various media [1]. On one hand, the use of interference between waves polarized in the plane of incidence has been shown to be effective in creation of

#135624 - $15.00 USD Received 28 Sep 2010; revised 28 Oct 2010; accepted 20 Dec 2010; published 5 Jan 2011

polarization micro-manipulators and optical tweezers. On the other hand, this is a vital step in optimal experimental investigation of optical currents in vector fields [2–5]. Besides, the study of spatial and temporal peculiarities of the motion of particles embedded in optical fields with various spatial configurations and with various scale distributions of the Poynting vector leads to new techniques for estimating the temporal coherence of optical fields [6].

Computation of the spatial distribution of the averaged Poynting vectors determining the forces affecting the microparticles and their movement is here performed following the algorithm proposed by M. Berry [1], who has shown that the vectorial force affecting a small conducting particle in an optical field is proportional to the Poynting vector. Besides, it is shown that the study of the motion of microparticles in inhomogeneously polarized fields provides reconstruction of the spatial distribution of the averaged Poynting vectors (i.e. the optical currents).

2. Two-wave superposition for changeable degree of coherence of one component

Superposition of two plane waves of equal amplitudes polarized in the plane of incidence (Fig. 1a) results in the distribution of the Poynting vector shown in Fig. 1b. Such distribution arises when the interference angle is equal to 90°, and the only periodical polarization modulation of the field (in the absence of intensity modulation) takes place in the plane of observation.

An analysis of the spatial distribution of the averaged Poynting vectors shown in Fig. 1b reveals the periodicity of this distribution, where the absolute magnitudes of the vectors are proportional to the lengths of lines shown in the figure. The lines corresponding to the singularities of the Poynting vector are shown in this figure by the indicated set of points [7–9].

A comprehensive explanation of the mechanisms for formation of such a distribution follows from considering both in statistical terms and with respect to the dynamics with the corresponding comments, which are formulated below:

1. Light energy transfer is modulated in time and in space, as it is illustrated in video fragments Media 1 and Media 2. Here, the vectors $\vec{E}$ and $\vec{H}$ of electric and magnetic fields, respectively, are shown in blue and violet, respectively, and the Poynting vector is shown in black. The directions of the spatial oscillations of this vector indicate the direction of light energy transfer.

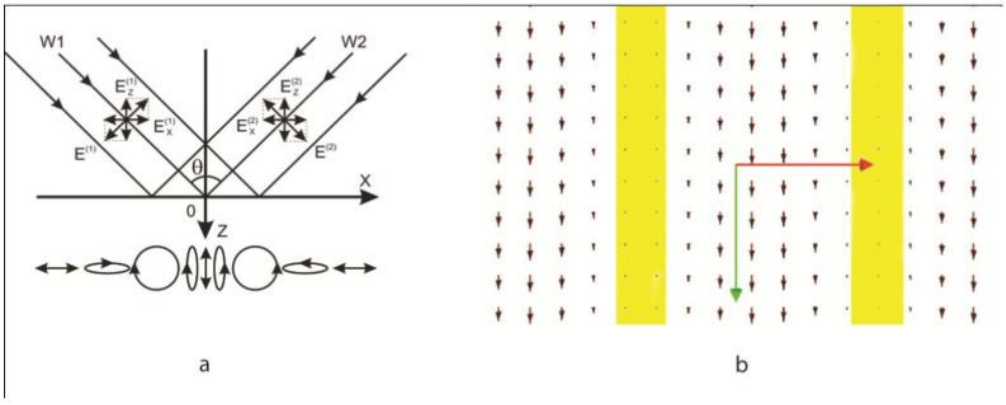

Fig. 1. (a) Superposition of plane waves of equal amplitudes, linearly polarized in the plane of incidence having an interference angle of 90°. Periodical spatial polarization modulation takes place in the plane of incidence. (b) Spatial distribution of the averaged Poynting vectors resulting from superposition of two orthogonally linearly polarized waves with an interference angle of 90°. Red and green axes (0.25 μm of length) correspond to x- and z-coordinates, respectively Media 1. Media 2. The points in the map of the averaged Poynting vectors correspond to the areas (indicated by yellow) through which energy transfer is absent.

#135624 - $15.00 USD Received 28 Sep 2010; revised 28 Oct 2010; accepted 20 Dec 2010; published 5 Jan 2011

Media 1 and Media 2 illustrate wave-like light energy transfer in a 2D field resulting from superposition of plane waves of equal amplitudes, orthogonally polarized in the plane of incidence with an interference angle of 90°. Energy transfer takes place along the bisector of the propagation directions of the two waves in the plane of incidence.

2. The spatial distribution of the averaged Poynting vectors (Fig. 1b) depicts the directions (trajectories) of energy transfer.

3. The yellow stripes in Fig. 1b indicate the regions where the Poynting vector magnitudes are close to zero. In points along the vertical line of the yellow stripes, the Poynting vector magnitude equals zero so that they form a singular manifold for the Poynting vector field. In these singular points the optical field intensity is non-zero but the energy does not moves. This follows from the fact that vector H vanishes due to interference in this arrangement (90°-superposition of plane waves) where strictly coaxial vectors of equal amplitudes and with opposite phases are associated with two superimposed plane waves

4. Homogeneous intensity distribution and periodical spatial modulation of the Poynting vector simultaneously realized in the analyzing area have previously been discussed within the framework of Refs [10,11]. Spatial polarization modulation in the analyzing area is caused by superposition of the E_x and E_z field components with a change of the phase difference from point to point (Fig. 1a). The photodetector only registers the intensity $I = \langle E_x^2 \rangle + \langle E_z^2 \rangle$. The sum of the average squared amplitudes of the electrical fields is constant in the analyzing area, though the state of polarization changes. The Poynting vector is defined by the vector product $\vec{S} = \frac{c}{4\pi}\left[\vec{E} \times \vec{H}\right]$. One observes the dependence of the result on the phase relation between vectors $\vec{E}$ and $\vec{H}$ through the vector magnitude and its direction. This relation changes from point to point in the analyzing area and results in polarization modulation. An obvious explanation for this follows from consideration of the vector product of the components of vector $\vec{E}$ (E_x and E_z components) with vector $\vec{H}$. Both the magnitudes of projections E_x and E_z and their phases change from point to point in the observation plane. As a consequence, the vector product as well as the Poynting vector changes.

Simulation of particle motion was carried out for conducting particles affected by the Poynting vector, in correspondence with Ref [1]. Two kinds of conducting particles were considered, *viz.* completely absorbing and completely reflected ones. The difference between absorbing and reflecting particles has been taken into account in computing the forces acting on a particle surface. For absorbing particles, the force acting on the surface point coincides in direction with the Poynting vector and is proportional it to its modulus. In contrast, for reflecting particle if $\vec{S}_1$ is the incident Poynting vector and $\vec{S}_2$ is the reflected Poynting vector, the force is directed along $\vec{S}_1 - \vec{S}_2$ and its numerical value is proportional to $\left|\vec{S}_1 - \vec{S}_2\right|$. The influence of the particles on the field itself and other fine effects were not taken into account due to complexity of the corresponding computations at this stage.

If one knows the forces $\vec{f}_i$ affecting the surface of spherical particle at points $\vec{r}_i = \left(x\ , y\ , z\ \right)$ measured from the center of mass, then its motion can be decomposed into sliding motion of the center of mass and rotational motion around the axis passing this center. The corresponding equations have the form:

$$m\frac{d\vec{v}_c}{dt} = \sum_i \vec{f}_i\ - 6\pi\eta R\vec{v}_c\,, \qquad (1)$$

#135624 - $15.00 USD Received 28 Sep 2010; revised 28 Oct 2010; accepted 20 Dec 2010; published 5 Jan 2011

$$0.4mR^2 \frac{d\vec{\Omega}}{dt} = \sum_i \left[\vec{f}_i \times \vec{r}_i \right] - \pi^2 \eta R^3 \vec{\Omega} \ . \qquad (2)$$

Here m and R are the mass of the spherical particle and its radius, respectively, η is the viscosity of the liquid, $\vec{v}_c$ is the velocity vector of sliding motion of the mass centre, and $\vec{\Omega}$ is the vector of angular velocity of the spherical particle. Initial conditions are $\vec{v}_c = 0$ and $\vec{\Omega} = 0$. The second term on the right side of Eq. (1) is the force due to the Stokes viscid friction. The second term on the right side of Eq. (2) is the momentum of force of viscid friction due to rotation.

Rotational motion of a spherical particle does not affect essentially its sliding motion. That is why it is not taken into account in simulation. The tracking of the particle motion was divided into small time intervals for which the resulting force was considered constant. Elementary motion of a particle was computed for these intervals using Eq. (1). The sum of elementary motions of a particle results in the trajectory of the particle. Interaction of colliding particles was assumed be elastic.

The results of simulating the motion of particles embedded in the field of the considered distribution of the Poynting vector is shown in Fig. 2 (see also Media 3). We have here assumed the particles to be absorbing and of size 0.1 μm. One observes that in the case of the distribution resulting from superposition of completely mutually coherent waves, the velocities of particle motion along the lines of maxima and zeroes of the Poynting vector are considerably different from one another. The particle size is here comparable with a half-period of the corresponding distribution, however, the resultant force giving rise to the particle motion along the lines close to the Poynting vector maxima exceeds the resultant force for lines close to the zeroes of the Poynting vector, as seen in Fig. 2 and Media 3.

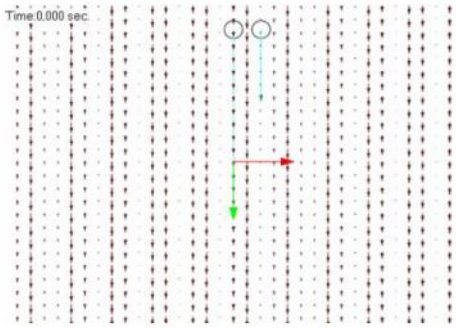

Fig. 2. Illustration of velocities of microparticles in a 2D distribution of the averaged Poynting vectors formed in arrangement Fig. 1a for completely mutually coherent waves. Red and green axes (0.5 μm of length) correspond to x- and z-coordinates, respectively. Media 3.

If the degree of mutual coherence of the superimposed waves equals 0.2, the spatial distribution of the averaged Poynting vectors becomes more homogeneous, the modulation depth decreases considerably, and the velocities of the microparticles become almost identical as shown in Fig. 3 and Media 4.

#135624 - $15.00 USD Received 28 Sep 2010; revised 28 Oct 2010; accepted 20 Dec 2010; published 5 Jan 2011

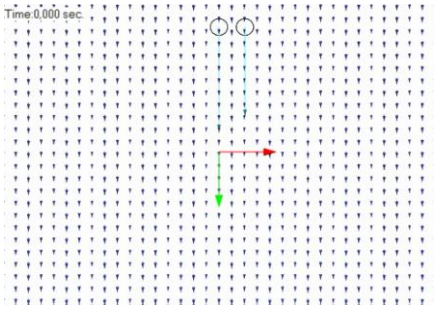

Fig. 3. Illustration of microparticles motion velocities in a 2D field distribution of the averaged Poynting vectors formed by the arrangement in Fig. 1 for a degree of mutual coherence of the components equal to 0.2. Red and green axes (0.5 μm of length) correspond to x- and z-coordinates, respectively. Media 4.

When the degree of mutual coherence equals 0.5, the relative velocities of the microparticles along the same trajectories are half compared with velocities in case of full mutual coherence of the superposed waves, see Fig. 4 and Media 5. One observes the dependence of the coherent properties of the superimposed waves on the motion of the microparticles with constant size and shape in media with constant viscosity. These differences in velocities of motion of microparticles may be explained physically in the following manner: Increasing the amount of incoherent radiation in the resulting field distribution causes a decrease of the modulation depth of the Poynting vectors spatial distribution, as well as in a decrease of the resultant force magnitude along the lines of energy transfer, which eventually induces the motion of the microparticles.

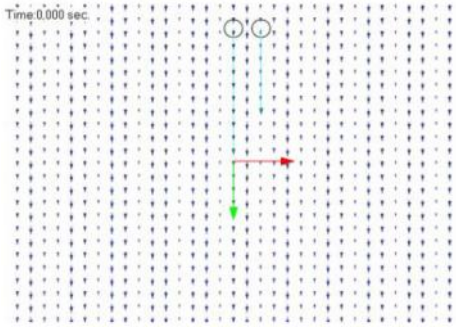

Fig. 4. Illustration of microparticles motion velocities in the 2D field distribution of the averaged Poynting vectors shown in Fig. 1 for the degree of mutual coherence of the components equal to 0.5. Red and green axes (0.5 μm of length) correspond to x- and z-coordinates, respectively. Media 5.

#135624 - $15.00 USD Received 28 Sep 2010; revised 28 Oct 2010; accepted 20 Dec 2010; published 5 Jan 2011

3. The superposition of four waves for changeable degree of coherence of one component

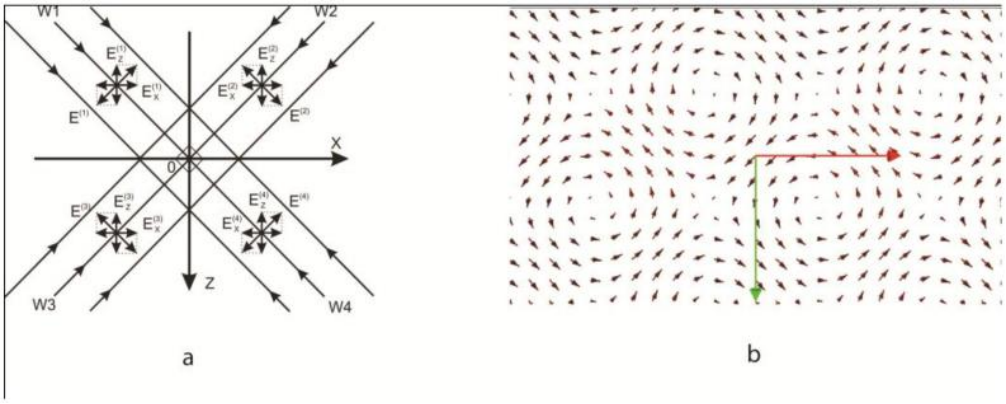

Fig. 5. (a) Arrangement of superposition of four plane waves. (b) 2D distribution of the averaged Poynting vectors resulting from the superposition of four waves shown in Fig. 5a. . Red and green axes (0.25 μm of length) correspond to x- and z-coordinates, respectively.

In the case of the superposition of four mutually coherent waves involving two sets of counter-propagating plane waves of equal intensities, linearly polarized in the plane of incidence and oriented at an angle of 90° with respect to each other, cf. Figure 5a, the electric and magnetic vectors of the resulting field are written in the form:

$$\vec{E} = \vec{E}^{(1)} + \vec{E}^{(2)} + \vec{E}^{(3)} + \vec{E}^{(4)}, \tag{3}$$

$$\vec{H} = \vec{H}^{(1)} + \vec{H}^{(2)} + \vec{H}^{(3)} + \vec{H}^{(4)}. \tag{4}$$

Here,

$$\vec{E}^{(i)} = E_x^{(i)}\vec{i} + E_y^{(i)}\vec{j} + E_z^{(i)}\vec{k}, \tag{5}$$

$$\vec{H}^{(i)} = H_x^{(i)}\vec{i} + H_y^{(i)}\vec{j} + H_z^{(i)}\vec{k}, \tag{6}$$

$$E_j^{(i)} = E_{j0}^{(i)} \exp\left[i\left(\omega t - k_j^{(i)} j + \varphi_0^{(i)} \right) \right], \tag{7}$$

$$H_j^{(i)} = H_{j0}^{(i)} \exp\left[i\left(\omega t - k_j^{(i)} j + \varphi_0^{(i)} \right) \right], \tag{8}$$

where $\vec{i}$, $\vec{j}$, $\vec{k}$ are x, y and z unit normal vectors, respectively, i = 1,2,3,4 is the number of the wave, $j = x,y,z$ are the vector components, $E_{j0}^{(i)}$ and $H_{j0}^{(i)}$ are amplitudes of the corresponding components of electrical and magnetic vectors, respectively, $k_j^{(i)}$ and $\varphi_0^{(i)}$ are the wave vector and initial phase of the corresponding plane wave, and $\vec{r}$ is the position vector.

We consider two configurations:

Initial phase of all four waves equals zero:

$$\varphi_0^{(1)} = \varphi_0^{(2)} = \varphi_0^{(3)} = \varphi_0^{(4)} = 0. \tag{9}$$

Initial phase of waves one to three equals zero, while the initial phase of the wave four is π :

$$\varphi_0^{(1)} = \varphi_0^{(2)} = \varphi_0^{(3)} = 0,\ \varphi_0^{(4)} = \pi. \tag{10}$$

Partial coherence of the beams is taken into account through the modulus of the complex degree of coherence [6].

#135624 - $15.00 USD Received 28 Sep 2010; revised 28 Oct 2010; accepted 20 Dec 2010; published 5 Jan 2011

An example of the spatial distribution of the averaged Poynting vectors is shown in Fig. 5b.

The 2D periodical distribution of the Poynting vectors is evident. As in the previous case, the lengths of the arrows in Fig. 5b are proportional to the local Poynting vector magnitudes. The nodal points in this distribution correspond to zero magnitudes of the Poynting vector, i.e. singularities of the Poynting vector. In the following simulation, the diameters of the particles are changed to be comparable with a half-period of the corresponding spatial distribution of the Poynting vector.

In order to compare the influence of the temporal and spatial parameters of coherence on the motion of the microparticles, we have analyzed maps of the averaged Poynting vector with a superposition of four plane waves over a large area. During this, we have tracked the microparticles' motion. This reveals the dependence of the microparticles' velocities on the phase difference of the superposing beams. So, in the case of pair-by-pair four opposite-in-phase superimposed beams, particles become motionless, cf. Figure 6. Here, "opposite-in-phase" describes the situation when the wave phases are described by Eq. (10). This follows from the presence of the minimum of the modulation depth in the spatial distribution of the Poynting vector. Gradually decreasing the degree of coherence of one of the superimposed beams causes revival of the particle motion with increased velocity as the degree of coherence of one of the beams decreases, see Fig. 7.

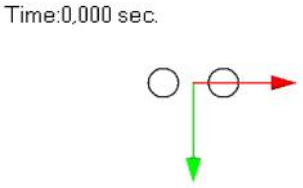

Fig. 6. Spatial distribution of the averaged Poynting vectors for four-wave superposition of components with initial phases from Eq. (9), illustrating a steady-state situation for the resulting field. (Time in sec.). Red and green axes (0.5 μm of length) correspond to x- and z-coordinates. Media 6.

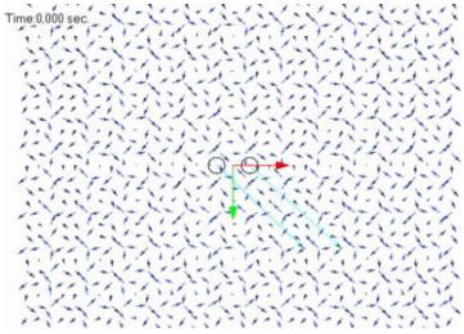

Fig. 7. Illustrating the movement of a microparticle when of one of four waves with a mutual degree of coherence of 0.5 with other three waves takes part in the forming of a spatial distribution of the averaged Poynting vectors. (Time in sec.). Initial phases defined from Eq. (9). Red and green axes (0.5 μm of length) correspond to x- and z-coordinates, respectively. Media 7.

#135624 - $15.00 USD Received 28 Sep 2010; revised 28 Oct 2010; accepted 20 Dec 2010; published 5 Jan 2011

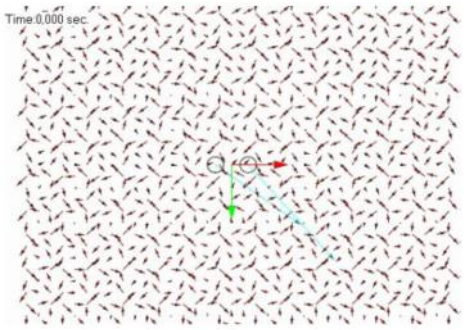

Fig. 8. Illustration of moving microparticles, when the spatial distribution of the averaged Poynting vector is formed by four mutually coherent waves with phases defined from Eq. (10). Time in sec.). Red and green axes (0.5 μm of length) correspond to x- and z-coordinates, respectively. Media 8.

If the phase relations between four superimposed beams are such that the modulation depth of the spatial distribution of the Poynting vector is maximal, the particle velocities will depend on the degree of mutual coherence between the interfering beams. This conclusion is supported by two video fragments corresponding to complete coherence of the beams (Fig. 8) and the situation when one of the beams is incoherent (Fig. 9). This situation is realized when two orthogonal systems of the standing waves are such that their maxima coincide. This case we refer to as co-phasing of waves.

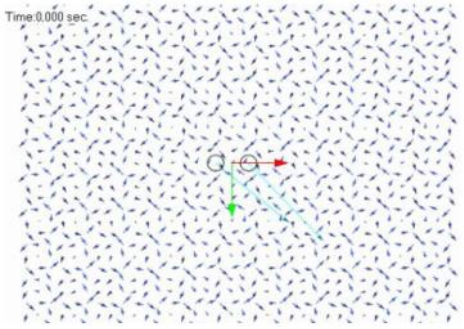

Fig. 9. Illustration of moving microparticles, when the spatial distribution of the averaged Poynting vector is formed by four beams, one of which is incoherent with respect to the other three. (Time in sec.). Initial phases defined from Eq. (10). Red and green axes (0.5 μm of length) correspond to x- and z-coordinates, respectively. Media 9.

It is worth emphasizing two issues for the case of superposition of four plane waves. First, the dependence of the depth of modulation for the distribution of the averaged Poynting vectors on the phase relation of superposing waves as illustrated in Figs. 6 and 8. It is here assumed that the phase relation between the superimposed waves is described by Eq. (9). Thus, the velocities of particles in such fields depend on the depth of modulation of the distribution of the averaged Poynting vector, as it is seen in Fig. 7. Second, the superposition of four waves linearly polarized in the plane of incidence results in forming so-called "cellular" structure in the resulting field distribution, which can be used for transfer (transporting) as an entity of the set of periodically positioned microparticles to a desired zone, see Fig. 10.

#135624 - $15.00 USD Received 28 Sep 2010; revised 28 Oct 2010; accepted 20 Dec 2010; published 5 Jan 2011

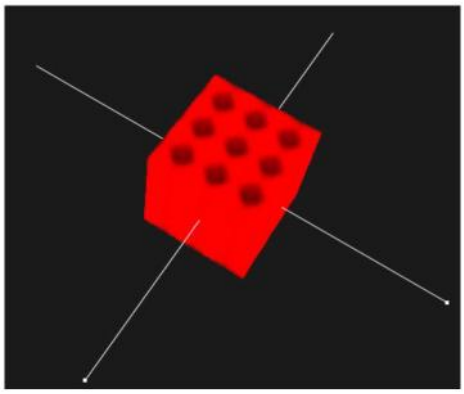

Fig. 10. “Cellular” distribution of the potential traps for microparticles in the case of superposition of four waves.

Here we represent the results of a more profound investigation of the peculiarities of motion of microparticles in order to reveal the coherent characteristics of the waves constituting certain spatial polarization distributions.

The use of strongly reflecting spherical test particles provides the means for more realistic notion on movement of particles in a field modulated in polarization in the incidence plane. Accordingly, the test particles are concentrated in zones (planes) of minima of the averaged Poynting vector and move along these planes, cf. Figure 11. This situation reflects in the most adequate manner the processes of particle movement in spatially modulated fields modulated with respect to polarization.

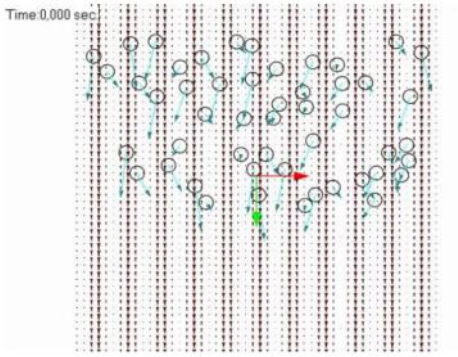

Fig. 11. Illustration of the direction and mechanism of energy transfer for superposition of two linearly polarized waves of equal intensity; here the waves are polarized in the plane of incidence, meeting at right angle. (Time in sec.). Red and green axes (0.5 μm of length) correspond to x- and z-coordinates, respectively. Media 10.

4. Experimental technique and results

Direct experimental verification of the results of computer simulation is rather difficult. The spatial period of the polarization distribution resulting from orthogonal superposition of plane waves is less than a wavelength of the laser radiation in the visible range. In this case, diagnostics of optical currents presumes the use of test particles (preferably spherical) of size much less than the period of polarization distribution. That is why, direct visualization and diagnostics of such particle currents is hampered.

For verifying the results of the computer simulations, we have studied experimentally the influence of the field resulting from superposition of two plane waves meeting at right angle with various combinations of their states of polarization on the test particles. The scheme for forming a controllable distribution is shown in Fig. 12. Two parallel, linearly polarized beams

#135624 - $15.00 USD Received 28 Sep 2010; revised 28 Oct 2010; accepted 20 Dec 2010; published 5 Jan 2011

converge at the focus of microobjective. According to [12], two quasi-plane waves are formed at the focus. To provide a right angle between the beam axes, we use an immerse oil microobjective 90x with NA 1.25. If the electrical vectors of two beams are parallel, the intensity distribution as a set of interference maxima and minima is formed in the area of superposition of such beams. We used radiation from a semiconductor laser RLTMRL-III-635 (λ = 635 nm). Therefore, the period of the interference pattern is 449 nm. For investigating the influence of this field distribution on the particles, the particles' size must be much less than the mentioned period. We have used spherical particles of hydrosol of gold with an approximate diameter of 40 nm. Hydrosol have been obtained following the standard technique [13], by mixing of chloroauric acid (H[AuCl4]) and sodium citrate (Na3Cyt).

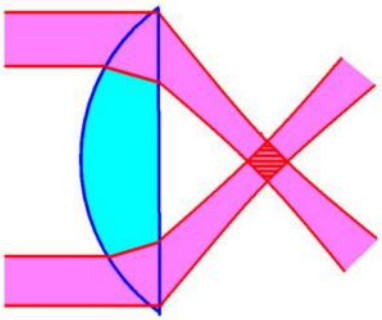

Fig. 12. Arrangement for forming the desired spatial interference distribution. Polarization of both crossed beams is linear, perpendicular to the figure plane.

Periodical intensity and Poynting vector distributions cause movement of the particles and formation of a periodical distribution of concentration of particles in the planes coinciding with the interference minima of the intensity distribution. These planes can be regarded as the analogy of crystallographic planes. Direct visualization of particles and their currents is hampered due to the small particle size. However, at planes of dense packing of particles self-diffraction takes place. We have observed this phenomenon for crossing angles of the two beams less than 40°. For right crossing angle between the beams, each of the self-diffracted beams propagate both along of and contrary to the propagation direction of the two superposing beams. Thus, it is impossible to discriminate between the initial and the self-diffracted beams. That is why, taking into account the Bragg law, we use a test laser beam with a different wavelength, λ = 532 nm for diagnostics of the periodical distributions of particles. To form the same interference distribution (with the period 449 nm) with this wavelength, the crossing angle of the two beams should be 72.6°. So, the angle of incidence of the probing beam must be 36.3° with respect to the bisector of the writing beams. In this case, the Bragg law is strictly fulfilled for the probing beam. The mentioned angles are the angles of propagation in the light-scattering media, in our case water.

The experimental arrangement is shown in Fig. 13. The radiation emitted from lasers L1 and L2 is linearly polarized in the plane perpendicular to the figure plane and passes through the telescopic systems TS1 and TS2, respectively, each of which are formed by two objectives with a micron-size diaphragms at the focuses. Two parallel beams of diameter 0.6 mm are formed in this arrangement. A beam-splitter BS divides a beam of a red laser into two beams, and the system of mirrors M2-M3-M4 provides strict parallelism between them. An intensity distribution with a set of planes of interference maxima and minima is formed at the back focus of microobjective MO1. Two slightly shifted beams from a green laser propagate parallel to the beams of the red laser. The external green beam is stopped by the screen S, while the inner probing beam passes the microobjective MO1 and falls at an angle 36.3° into the area of the interference extrema. The diameters of the focused beams for the red and green lasers are approximately 12 μm and 10 μm, respectively. Glass cuvette C with gold hydrosol is placed

#135624 - $15.00 USD Received 28 Sep 2010; revised 28 Oct 2010; accepted 20 Dec 2010; published 5 Jan 2011

in the area of the interference pattern. The thickness of the cuvette walls is 0.15 mm, and the thickness of the swept volume is 18 μm. Oil immersion with index of refraction 1.515 is placed between microobjectives MO1 and MO2. Microobjective MO2 is used for adjusting the optical arrangement and transmit the light onto the periodical distribution of gold particles. This radiation passes the interference filter IF with the maximal transmittance at 532 nm (excluding the radiation of the red laser), 0.7mm-diam diaphragm D1, microobjective MO3, microdiaphragm D2, and eventually falls on the photodetector PD. The signal from the photodetector is sent through an amplifier A and an ADC to a PC.

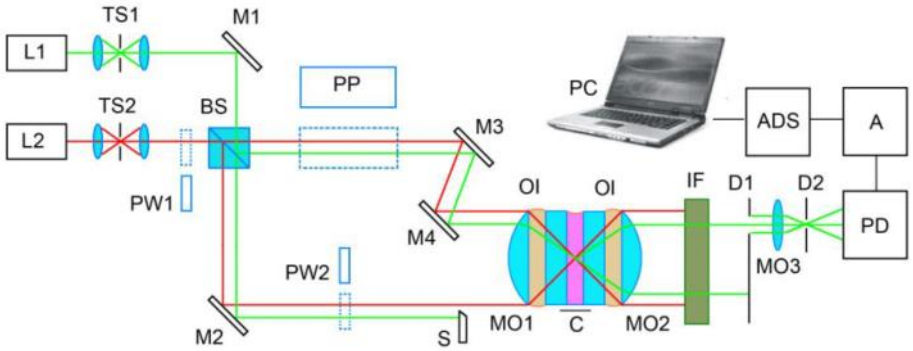

Fig. 13. Experimental setup: L1, L2 - lasers, TS1, TS2 - telescopic systems, M1, M2, M3, M4 - mirrors, PW1, W2 - half-wave plates for λ = 635 nm, PP - plane-parallel plate, MO1, MO2, MO3 - microobjectives, C - cuvette with gold hydrosol, IF - interference filter at λ = 532 nm, D1, D2 - diaphragms, S - opaque screen, PD - photodetector, A - amplifier, ADC - analog-to-digital converter, PC - computer.

The optical path lengths of the two legs in the interferometer BS-M2-M3-M4-MO2 are strictly identical. As a result, the two beams from the red laser are mutually coherent and interfere at the focus of the micro-objective MO2. Placing a perfect plane-parallel plate PP of thickness 19 mm into one leg in the interferometer leads to disappearance of interference, as the corresponding optical path difference exceeds the coherence length of the red laser. It is important that the introduction of the plate PP must not be accompanied with shifting beams in the interferometer. In this manner, one can control the appearance and disappearance of interference extrema at the focus of MO1.

The experimental technique used here is as follows. If radiations from lasers L1 and L2 are linearly polarized in the plane perpendicular to the figure plane, one records the signal from the photodetector PD, cf. Figure 13. We used a photomultiplier with and without a plane-parallel plate PP mounted as previously described. In the first case, the periodical interference planes are absent; so, the diffracted light is absent also. The signal from a PD is caused by Bragg scattering of the probing beam from the homogeneous distribution of gold particles. Removal of the plate PP results in an increased signal from the photodetector. This proves the formation of a periodical spatial distribution of gold particles and appearance of the diffracted probing beam (Fig. 14a). The diffracted signal appears for the radiation power of the red laser exceeding 2 mW. However, for radiation power exceeding 50 mW, non-linear effects occur in the light-scattering medium. As a result, gold particles absorb radiation and the heated environment will act as a thermal lens. Thus we have carried out our experiments with radiation power of 5 mW for the red laser. The power of the probing beam was 0.5 mW, thus not affecting the gold particles. The experimental results shown in Fig. 14a, where radiations of lasers L1 and L2 are polarized in the plane perpendicular to the figure plane, support the computer simulations.

#135624 - $15.00 USD Received 28 Sep 2010; revised 28 Oct 2010; accepted 20 Dec 2010; published 5 Jan 2011

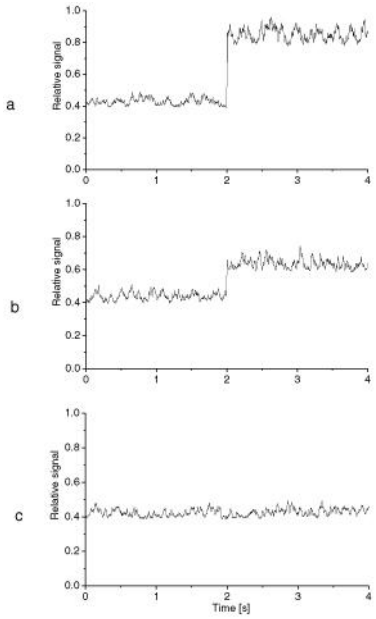

Fig. 14. Relative signal for a photodetector (a plate PP is inserted on 2 sec and then removed) in the case when radiation of red laser is linearly polarized: (a) both beams are polarized in the plane perpendicular to the figure plane; (b) both beams are polarized in the figure plane; (c) one beam is polarized at the figure plane, while another one is polarized perpendicularly to this plane.

If two beams of red laser are polarized in the figure plane (half-wavelength plate PW1 for $\lambda = 635$ nm is inserted), the signal at the photodetector output with and without plane-parallel plate is shown in Fig. 14b. The diffracted probing beam is present, but is approximately of half the intensity in comparison with the former case illustrated by Fig. 14a. This experimental result is also in accordance with the result of computer simulation. From this figure one can see that the spatially modulated in polarization field (in the plane of incidence) is correlated with concentration of the test particles at the planes of minima of the averaged magnitude of the Poynting vector, and particles move along these planes.

If two beams form the red laser are linearly polarized, but one of them is polarized in the figure plane while another one is polarized perpendicularly to this plane (a half-wave plate PW2 for $\lambda = 635$ nm is inserted), the diffracted probing beam is absent, Fig. 14c. This shows that at the focal point where the beams from the red laser are superimposed, the periodical distributions of gold particles are absent. This is supported by computer simulation, see Fig. 15. This media file shows that discrimination of any periodical structure of spatial concentration of particles is absent in the averaged Poynting vector causing the modulation of spatial particle concentration. In other words, there are no ordered optical currents being noticed by optical diagnostics, as it has been evident in the previous case.

#135624 - $15.00 USD Received 28 Sep 2010; revised 28 Oct 2010; accepted 20 Dec 2010; published 5 Jan 2011

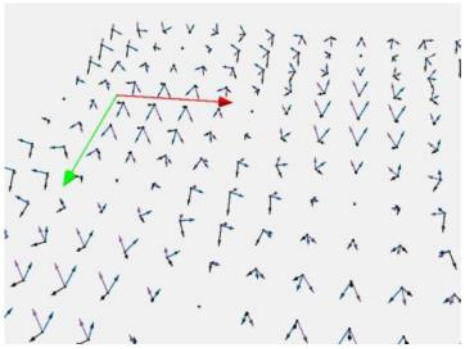

Fig. 15. Illustration of the directions of oscillations of the vectors $\vec{E}, \vec{H}, \vec{S}$ for superposition of two waves of equal intensity one of which is linearly polarized in the plane of incidence and another perpendicularly to this plane. The crossing angle between the two beams equals 90°. Red and green axes (0.25 μm of length) correspond to x- and z-coordinates, respectively. Media 11.

5. Conclusions

The motion of micro- and nanoparticles in a field without intensity modulation, but only due to polarization modulation causing the spatial modulation of the Poynting vector facilitates the creation of pure polarization micromanipulators and tweezers. Temporal and spatial peculiarities of the particles' motion in optical fields with spatial modulation of the averaged Poynting vector (depending on the degree of mutual coherence of superpose waves) opens up new feasibilities for the use of such field characteristics and the parameters of microparticles motion for estimating the temporal coherence of the tested field. Initial experimental results prove these conclusions. For the first time, we have demonstrated the possibility of using the influence of only the polarization on the formation of optical currents in liquids by the use of the principles of spatial polarization modulation in the observation plane. Besides, we have shown the possibility of diagnostics of optical currents using test particles of nanoscale.

Acknowledgement

The authors are grateful to Prof M. Berry, Prof S. Odoulov and Dr A. Shumelyuk for fruitful discussion and useful suggestions on this study.

#135624 - $15.00 USD Received 28 Sep 2010; revised 28 Oct 2010; accepted 20 Dec 2010; published 5 Jan 2011